Analysis of the entire surge cycle of a multi-stage high-speed compressor

By S. Teramoto†

1. Motivation and objectives

Both surge and rotating stall are flow instabilities observed at the low mass flow side of the compressor operating range. Rotating stall is a phenomenon in which a part of a cascade stalls to form a stall cell that rotates circumferentially. In surge, the stall of a cascade makes the entire compression system unstable and the mass flow rate oscillates violently (Greitzer (1976)). Surge forces the undesirable shutdown of the engine. Furthermore, unsteady blade loading, and rubbing between the casing and the rotor blade and burning of the blades often results in mechanical damage to the compressor. Surge is a phenomenon that must be avoided at all costs, and it therefore defines the operating range of a compressor. Surge is an important issue with regard to the development of a compressor, and hence the cause of surges or the reason for stalls has always been the subject of active research. Camp & Day (1998) measured the velocity fluctuation of a low-speed axial compressor at several circumferential locations, studying the disturbances that appear at the initial stage of surge inception and reporting that a stall cell appears before the surge. The development of the stall cell leads to stall of the entire cascade, and it causes the compressor surge.

Two types of rotating stalls are reported in the literature: One is modal stall, in which a relatively large stall cell composed of several cascade passages appears at the early stage of the rotating stall; the other is spike stall, in which the rotating stall starts from the stall of one cascade passage. Sekido *et al.* (1984), Sasaki & Takata (1981) studied the influence of the radial velocity profile upon the growth of circumferential disturbances. Furthermore, Moore & Greitzer (1986) analyzed the stability of circumferential disturbances, showing that the growth of circumferential disturbance leads to modal stall. Indeed, this growth in circumferential disturbance and the subsequent modal stall are also reported in measurements of wall pressure fluctuations in high-speed compressors (Day & Freeman (1994)).

Based on the idea that increased circumferential disturbance leads to modal stall, Day (1993) and Paduano *et al.* (2001) experimentally demonstrated active control of surge. They introduced a circumferential disturbance that offsets the disturbance observed in the compressor, showing that the surge margin is increased with active control. Recently, the spike stall has been studied using large-scale unsteady CFD in connection with clearance flow (Hah *et al.* (2006)).

These studies provide much useful knowledge regarding surge inception, but detailed information about the flowfield during surge is very rare, especially in relation to practical, high-speed compressors. There has been little discussion about the correlation between axial disturbances, circumferential disturbances, the performance of each stage, and the cascade flowfield. A lack of unsteady stage performance data also results in the

† Current Address: University of Tokyo, Japan

use of an expedient model in stability analysis. For example, many stability analyses of modal stall presume that unsteady stage performance is solely determined by parameters at the cascade inlet and time delay.

The purpose of the present study is to numerically simulate the entire surge cycle and obtain detailed information about the time history of the entire flowfield that cannot be obtained by experimental or theoretical analysis. This information will more clearly elucidate the processes surrounding surge inception.

2. Numerical methods

2.1. *Geometry and flow conditions*

This study examines the core of a PW6000, which consists of a high-pressure compressor (HPC), a high-pressure turbine (HPT) and a combustor. Essentially, this is the same engine that was studied by Medic *et al.*, 2007. The HPC has a strut, an IGV, five stages and the HPT, which is composed of one stage (Fig. 1). The combustor has a liner, but other components such as the fuel nozzle, the swirler and the dilution air ports were omitted for simplicity. The work fluid is assumed to be pure air throughout the computational domain, and the combustion at the combustor is not modeled but instead a heat source is introduced at the shaded area in Fig.2. In this region, the source term Δq determined from the following equation is added at the right hand side of the energy equation

$$\Delta q_{ijk} = \frac{\max(0, \rho_{ijk}\vec{u}_{ijk}\vec{S}_{ijk})\Delta Q_{total}}{\Sigma_i\Sigma_j\Sigma_k \max(0, \rho_{ijk}\vec{u}_{ijk}\vec{S}_{ijk})}$$

where, $\rho_{ijk}, \vec{u}_{ijk}, \vec{S}_{ijk}$ represent the density, the velocity vector and the area vector normal to ξ-constant the plane at each grid point. ΔQ_{total} is the total heat input. The mass flow rate at the HPC is controlled by adjusting the heat input. Bleed at the HPC and cooling air at the HPT are both ignored.

The mechanical shaft rotation speed is the same as in Medic's analysis. The total pressure, total temperature and flow angle at the inlet of the HPC, as well as the static pressure at the exit of HPT, are fixed to Medic's result.

2.2. *Grids*

These days, $3\times10^6-10^7$ grid points per passage are usually used for numerical simulations of cascade stall. Each stage of the modern HPC typically has 100 blades, so the total passage of a 5-stage HPC reaches 1,000. If the grid for the current simulation had $3 \times 10^6 - 10^7$ grid points per passage, the total grid points would be $3 \times 10^9 - 10^{10}$.

The typical period of the surge cycle is 50 rotor revolutions; therefore, the entire computational time must be set to the duration of a minimum of 100 rotor revolutions. When the time step is set to be 1/100 of the blade passing time, it will take 100 time steps to advance one blade spacing. Considering that each stage has 100 blades, the total computational steps can reach 10^6. Such large-scale computation is impossible, even with today's computer technology. For this reason, a much coarser grid will be used in the current study, as this allows for more affordable computational costs.

The current study focuses on phenomena that have a length scale ranging from the length of the entire compressor to the thickness of the separation region or the size of the tip clearance flow. Consequently, the smallest scale that must be resolved should be about 1/20 of the chord length and the number of grid points required for each direction

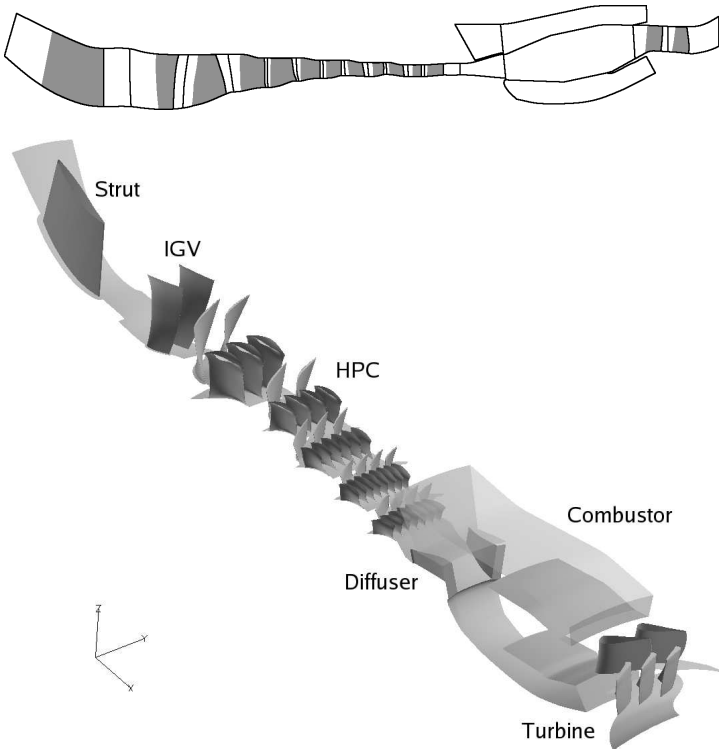

FIGURE 1. Geometry of the computational model.

will be about 50. Therefore, the minimum number of grid points per passage would be 10^5. The computational domain is also limited to a 20° sector assuming periodicity. Then the final grid point is reduced to 5×10^6. Flow separation resolved on such a coarse grid may not be "physically correct," but phenomena that have a length scale longer than the separation region will be resolved correctly with this grid. Therefore, it is still meaningful to discuss how the separation of the cascade influences the whole compressor.

Use of the sector computational domain with a periodic boundary condition introduces another uncertainty in the numerical result in that each rotor stage has only 2–4 passages and the stator stage has 1–8 blades within the computational domain. It is unknown whether rotating stall appears in such a small computational domain.

2.3. *Numerical schemes*

The code used in this study is a finite volume compressible RANS solver SUmb, which has been used in the analysis of the PW6000 at Stanford's Center for Turbulence Research.

2.4. *Initial condition and mass flow control*

First, a steady result with the mixing plane is achieved for several heat input values until the HPC reaches the numerical stall point. The steady result at the stall point is used as an initial condition for unsteady simulation with sliding mesh.

The numerical solutions near the stall point do not converge to steady states, as the combustor has large volume and the flowfield in it is essentially incompressible. Therefore, simulations of the HPC alone with the static pressure fixed at the diffuser exit are carried out to evaluate steady HPC characteristics.

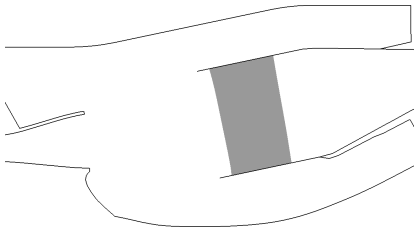

FIGURE 2. Heat source at the combustor.

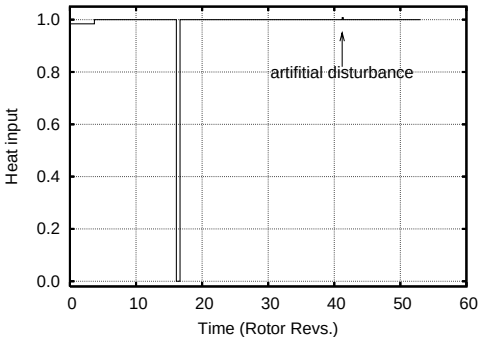

FIGURE 3. Time history of the heat input.

During the unsteady simulation, the heat input at the combustor liner is gradually increased to reduce the mass flow rate, then it is kept constant after 3.5 rotor revolutions, with the exception of 16.0 to 16.6 rotor revolutions. The mass flow rate at the combustor is close to zero during this period, so the heat input is set to zero in order to avoid divergence of the temperature. Note that the heat input was increased by 0.8% for a short period between 41.1 and 41.3 rotor revolutions in order to introduce the initial disturbance as a means of triggering Helmholtz oscillation. See Fig. 3 for the time history of the heat input.

3. Results

All the data shown hereafter, except that found in Fig. 9, were preprocessed with a low-pass filter to eliminate the Blade Passing Frequency (BPF) component. All the physical properties are non-dimensionalized using properties at the peak efficiency condition.

3.1. *Surge cycle*

The time histories of the mass flow rate at the compressor exit and the combustor pressure are shown in Fig. 4. The system falls into the first surge cycle at 8.4 rotor revolutions. The mass flow rate and the pressure then start to decrease simultaneously. The mass flow rate reaches zero at 8.8 rotor revolutions and the flow is reversed until 16.5 rotor revolutions. The positive flow recovers with a slight overshoot afterward and the flow rate returns to its pre-surge value at 25 rotor revolutions. The recovery of the combustor pressure is much slower than the mass flow rate, reaching its pre-surge value at 35 rotor revolutions.

The mass flow rate and the combustor pressure remain constant for a time, but they start oscillating immediately after the heat input disturbance is introduced at 41.1 rotor revolutions. The amplitude of the oscillation gradually develops and the second surge cycle begins at 50 rotor revolutions.

The trends of the mass flow rate and the combustor pressure shown in Fig. 4 are essentially the same as those reported in Fig. 3 of Day's study (Day(1994)). The key features of the surge are well reproduced in the current simulation.

3.2. *Disturbances at stall inception*

Figure 5 shows the time histories of mass flow at each rotor inlet during surge inception (3.5–8.5 rotor revolutions). Two types of fluctuations are observed: (1) 0.8 rotor revolu-

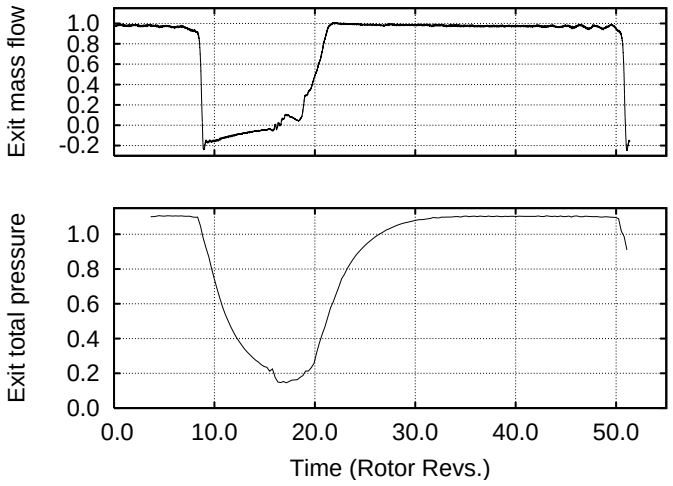

FIGURE 4. Surge cycle. Top: compressor exit mass flow rate. Bottom: combustion chamber pressure.

tions (cycle oscillations) at the front stages (Fig. 5(a) 1RB and 2RB) and (2) 1.5 rotor revolutions (cycle oscillations) at the rear stages (Fig. 5(b), 3RB, 4RB, 5RB).

In Fig. 5(b), T_1 and T_2 indicate the local minima of 1.5 rotor revolutions oscillations, and T_4 is the moment when the mass flow rate falls below the previous minimum mass flow rate. T_3 is the moment when the mass flow departs from 1.5 rotor revolutions oscillations. The downward arrows in Fig. 5(a) denote peaks of 0.8 rotor revolutions oscillations.

The peaks of 0.8 rotor revolutions oscillations for 1RB appear after the peaks for 2RB, showing that the disturbance propagates upstream. The propagation velocity estimated from the time difference between the peaks is approximately 140 m/s. The 0.8 rotor revolutions oscillations are a disturbance that corresponds to $u - c$.

On the other hand, 1.5 rotor revolutions oscillations at the rear stages fluctuate at the same phase within the three cascades. There is also no disturbance propagating axially at the rear stages in history of static pressure, as shown on the left in Fig. 8. Because the three rear stages oscillate with the same phase, the histories of the mass flow and the pressure at the exit of the last stage (mass flow at the compressor exit and combustor pressure) will be discussed further as a means of understanding these 1.5 rotor revolutions cycle oscillations. p

When we consider a system with an air column that has a mass of m, a cross-sectional area of S, and a chamber with a volume of V and a pressure of p_c as shown in Fig. 6(a), the air column velocities v and p_c are described by the following equations:

$$\frac{dp_c}{p_{c0}} \simeq -\gamma \frac{dV}{V_0} = -\gamma \frac{Sv}{V_0} dt \tag{3.1}$$

$$\frac{dv}{dt} \simeq \frac{S(p_c - p_{c0})}{m}. \tag{3.2}$$

Therefore, time derivatives for p_c and mass flow rate m are described as follows:

$$\frac{dp_c}{dt} \simeq -\gamma \frac{\dot{m}}{\rho V} p_{c0} \tag{3.3}$$

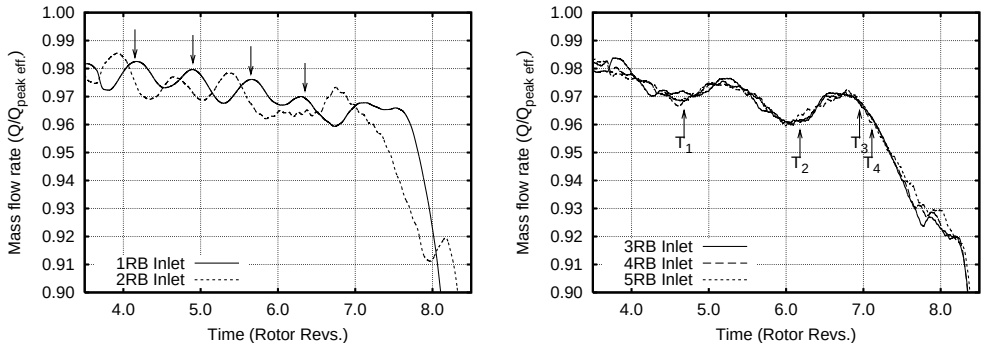

(a) Front stages (1RB, 2RB) (b) Rear stages (3RB, 4RB, 5RB)

FIGURE 5. Mass flow at each stage.

$$\frac{d\dot{m}}{dt} = \rho S \frac{dv}{dt} \simeq \frac{\rho S^2 (p_c - p_{c0})}{m}. \tag{3.4}$$

The actual time histories of the mass flow rate at the compressor exit and the combustion chamber pressure, as well as their time derivatives, are plotted in Figs. 6(b) and 6(c). The dashed line in the figures denotes gradients predicted from Eqs. (3.3) and (3.4). Here m, S and p_c are approximated as the mass of the air contained between IGV and 5SV, the corss sectional area at the diffuser exit and the combustion chamber pressure. During the period from time T_1 to time T_2 the mass flow rate decelerates when the chamber pressure is high (Fig. 6(b)), and the derivative of the chamber pressure is proportional to the mass flow rate (Fig. 6(c)). Fluctuations at the rear stages during this period follow Eqs. (3.3) and (3.4) for the most part. Consequently, the oscillation at the rear stages can be defined as Helmholtz oscillation.

After the time T_4, when the system falls into surge, the mass flow rate continues to decrease at a constant rate despite the decrease in chamber pressure. Meanwhile, the derivative of chamber pressure is still proportional to the compressor exit mass flow rate.

The following possible surge inception scenario can be derived from the above observation:

Before time T_3, the derivative of the mass flow is proportional to the chamber pressure and the derivative of the chamber pressure is proportional to the mass flow. Under such circumstances, both the mass flow and the chamber pressure fluctuate around the equilibrium point. relationship, the mass flow decreases more than that expected from pressure difference, and the excessive decrease of the mass flow push the compressor deeper into surge, resulting in much less discharge pressure, and then the mass flow then begins to decrease monotonically.

Thus, deviation of the $\frac{d\dot{m}}{dt}$-p_c curve triggers the surge. Necessarily, there should be some explanation for the cause of the deviation of the $\frac{d\dot{m}}{dt}$-p_c curve at time T_3.

3.3. *Cascade performances*

Figure 7 shows axial velocity contours at time T_3. It is almost impossible to discuss a complicated unsteady flowfield only with only such a picture, so the flowfield will be discussed with integrated cascade performances hereafter.

The time histories of the cascade performances are plotted in Fig. 8. From the stage static pressure ratio on the right, it can be seen that the pressure ratio for 3RB and 5RB

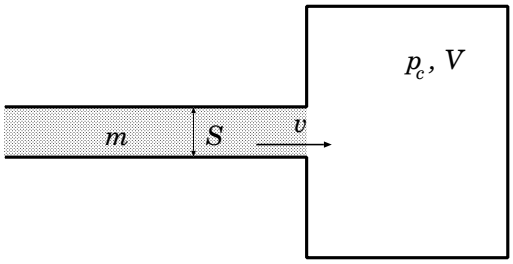

(a) Helmholtz oscillation

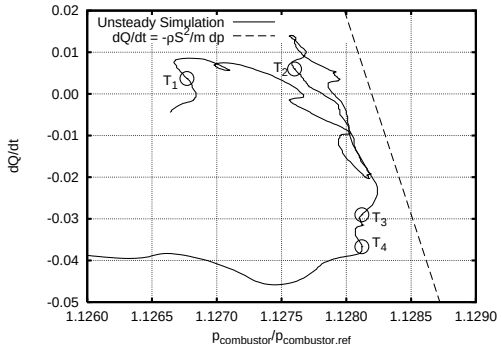

(b) $\frac{d\dot{m}}{dt}$ vs p_c

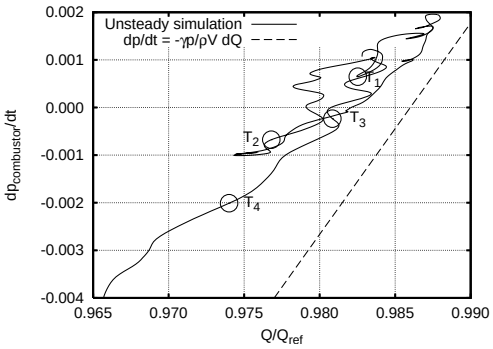

(c) $\frac{dp_c}{dt}$ vs $\dot{m}$

FIGURE 6. Mass flow and pressure at the compressor exit.

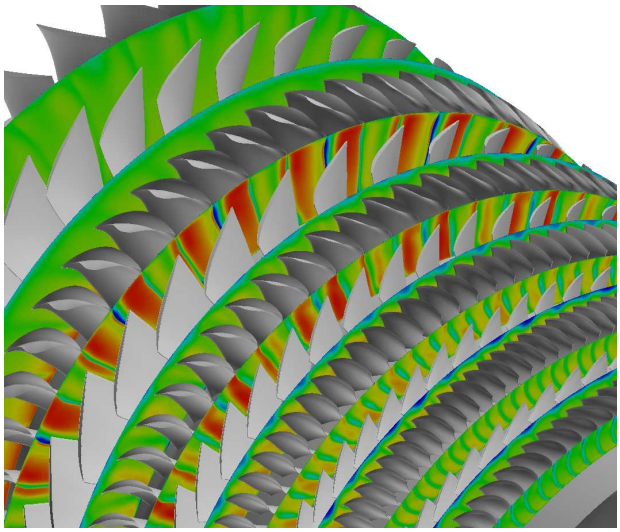

FIGURE 7. Axial velocity contours at time T_3.

decreases significantly at T_3, or 7.0 rotor revolutions. The histories of the tip velocities in Fig. 9 show that a velocity deficit at the tip region of 5RB enlarges at time T_3, indicating that 5RB stalled at the tip. On the other hand, there is no sign of tip stall in 3RB (Fig. 9(b)). Therefore, the deviation of the $\frac{d\dot{m}}{dt}$-p_c curve, that induced the surge is mainly caused by the tip stall in 5RB.

Next, interactions between each stage are discussed as they relate to the stage inlet static pressure, which is plotted on the left in Fig. 8. The following can be determined from Fig. 8:

• Pressure fluctuation related to the 0.8 rotor revolution cycle oscillation is observed at the front stages. The amplitude of the oscillation increases as it propagates upstream.

• In Fig. 5, the amplitude of mass flow fluctuation for the 1.5 rotor revolution cycle oscillation is almost the same as that for the 0.8 rotor revolution cycle oscillation however, pressure fluctuation corresponding to the 1.5 rotor revolution cycle oscillation is hardly detectable in Fig. 8 left.

• The pressure deviation caused by 5RB's stall at time 7.0 rotor revolutions is very small compared to the fluctuation at the front stages .

All the three phenomena, specifically the 0.8 rotor revolution cycle oscillation, the 1.5 rotor revolution cycle oscillation and the cascade stall, influence the pressure distribution. However it is found that the pressure distribution is mostly determined by the 1.5 rotor revolution cycle oscillation, which is the disturbance propagates upstream.

In order to understand the 1.5 rotor revolution cycle oscillation, the time histories of the mass flow and the pressure ratio of 3RB are shown, along with the characteristic curve, in Fig. 10. Fluctuations of the mass flow and the pressure ratio are both superposition of 0.8 rotor revolution cycle oscillation and 1.5 rotor revolution cycle oscillation, but the former is dominant in the pressure ratio, and the latter is dominant in the mass flow. The amplitude of 0.8 rotor revolution cycle oscillation in the mass flow rate is approximately 0.01 in non-dimensional units. The gradient of the characteristic curve during the oscillation is about $0.015/0.04 \simeq 0.38$, therefore the amplitude of the pressure ratio expected from the characteristic curve is 0.0038. However, the actual amplitude of the pressure ratio fluctuation is approximately 0.01, more than double of the expected value. This means that the loading (or adverse pressure gradient) of a cascade in an unsteady environment can be more severe than in the steady condition due to the transient interaction of the stages.

3.4. *Delay time*

Considering that cascade loading is largely influenced by axial disturbances propagated inside the compressor, it is important to model unsteady stage performance in order to predict the behavior of a compressor that may surge.

As previously mentioned, unsteady stage performance is usually modeled by considering steady performance and time delay, thus the correlation between the inlet mass flow rate and the stage pressure ratio is discussed in this section. In Fig. 11, characteristic curves are plotted at the top and time histories of the inlet mass flow rate and the stage pressure ratio are plotted at the bottom. The plot shows only four representative cascades. Two of the characteristic curves have positive slopes immediately preceding the surge while the other two exhibit negative slopes.

As for 1RB, the slope of the characteristic curve is negative, meaning that the peaks of the mass flow rate curve should match with the local minima of the pressure ratio curve if the delay time is zero. At the bottom of Fig. 11(a), the peak of the mass flow rate (represented by a dashed line) appears after the minima of the pressure ratio (represented by a solid line), therefore the delay time for 1RB is negative. As shown in Fig. 5(a), the fluctuation at 1RB is mainly caused by the propagation of disturbance from the downstream stages. Hence, the variation of the exit properties precedes that of the inlet properties, indicating that the negative delay time at 1RB is a result of the upstream propagation of disturbance. The slope of 2RB's characteristic curve is positive, so the

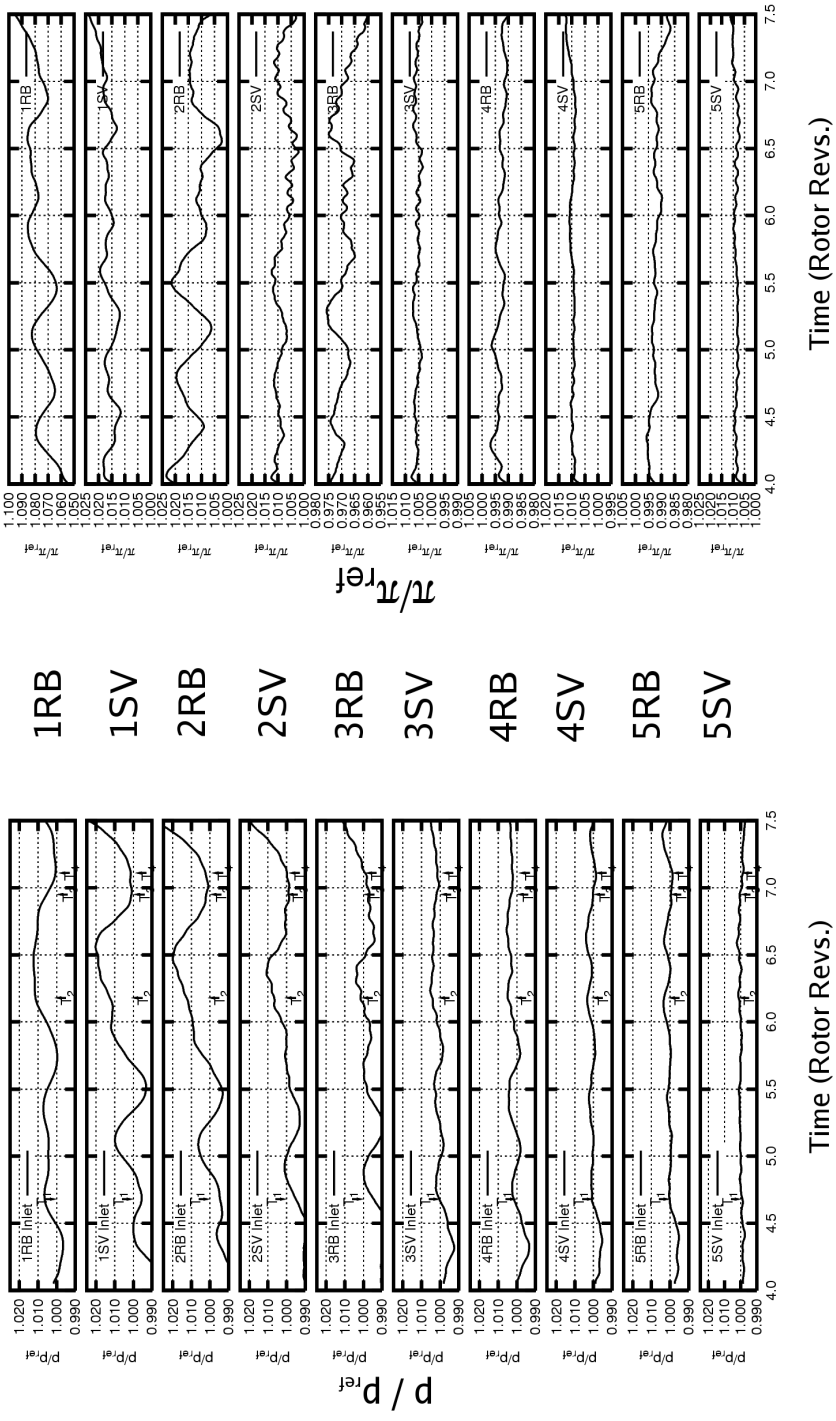

FIGURE 8. Cascade performance (left: inlet static pressure, right: static pressure ratio).

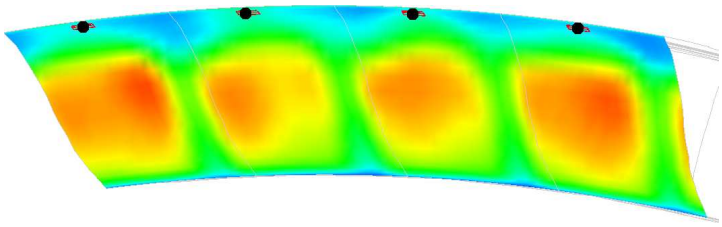

(a) 5RB exit axial velocity contour. Black dots denote points where the velocities are plotted.

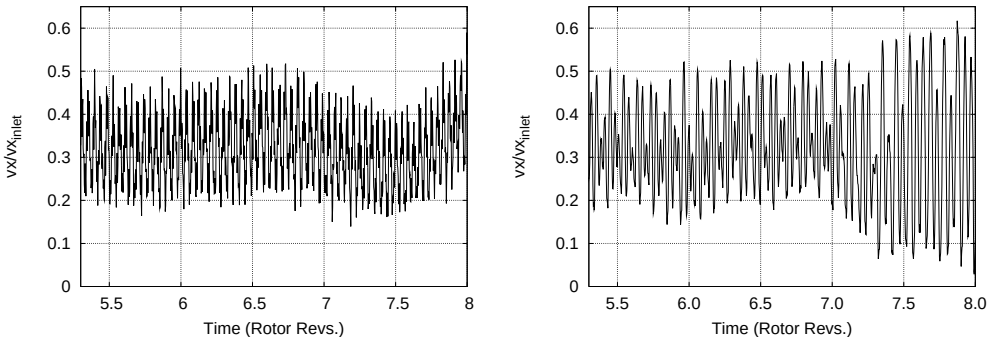

(b) 3RB (c) 5RB

FIGURE 9. Rotor tip velocity (3RB, 5RB).

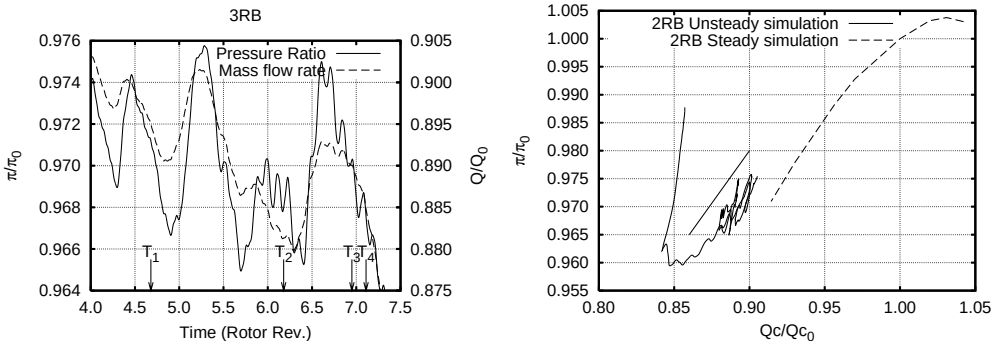

(a) Histories of pressure ratio & mass flow rate. (b) Characteristic curve.

FIGURE 10. 3RB characteristics.

peak of the pressure ratio corresponds to the peak of the inlet mass flow. The peak of the mass flow precedes that of the pressure ratio at the bottom of Fig. 11(b), so the delay time is positive despite the fact that the upstream propagation of disturbance is still dominant in this stage. The delay time of 4SV, which has a negative curve slope, is negative. For 5RB, which triggered the surge, no clear phase-lag between the mass flow rate and the pressure ratio is observed at the bottom of Fig. 11(d).

After comparing all 10 cascades, no correlation was found between the sign of the delay time and other parameters such as the slope of the characteristic curve, the position of the stage (front or rear) or the type of blade (rotor or stator). With regard to a multi-stage high-speed compressor, the unsteady cascade performance cannot be described by

a simple model that considers steady cascade performance and delay time. Disturbances propagating axially inside the compressor largely influence the unsteady cascade characteristic, so the effect of this unsteady cascade necessarily needs to be considered when predicting the unsteady performance.

3.5. *Stall criteria*

Unsteady cascade performance is usually modeled by considering steady performance determined solely by inlet parameters together with time delay. However, discussions so far have revealed that unsteady cascade performance is governed not only by local parameters, but is also also due to the transient interaction of the stages.

In the same way, the stall limit of a cascade cannot only be determined by local parameters. The incidence-pressure ratio correlation and the mass flow-pressure ratio correlation of 5RB are plotted in Fig. 12. Here, the incidence is the reltive flow angle evaluated from mass-averaged meridional velocity and circumferential velocity. Both the stage pressure ratio and the mass flow rate are non-dimensionalized using properties of the peak efficiency condition. Cascades at steady conditions stall when the mass flow falls below the critical mass flow or the incidence exceeds the critical incidence. However, the incidence at which the cascade stalled between T_3 and T_4 was below the maximum incidence during oscillation, and the mass flow between T_3 and T_4 was above the minimum mass flow during oscillation.

In Fig. 11(d), 5RB's pressure ratio oscillates at the period of 0.8 rotor revolutions, and the pressure ratio is at peak when the cascade stalls at time 7.0 rotor revolutions.

These results imply that a cascade with an unsteady inlet or outlet condition can stall with an incidence smaller than the maximum incidence or with a mass flow larger than the minimum mass flow rate, and the difference between steady and unsteady stall characteristics can be attributed to the fluctuation of stage loading due to transient interaction of the stages.

4. Summary

Surge of a multi-stage high-speed compressor was numerically simulated, and the entire surge process — from surge inception to the second cycle — was studied.

At the inception, two types of fluctuation were observed: One is an upstream propagation of disturbance and the other is Helmholtz oscillation. Helmholtz oscillation was dominant at the rear stages and triggered the surge. Indeed, at the moment the mass flow-discharge pressure correlation deviated from the Helmholtz correlation, the system surged.

In the current study, the key factor influencing an alteration of the mass flow-discharge pressure correlation was 5RB's tip stall. This cascade stalled at an incidence lower than the maximum incidence and at a mass flow higher than the minimum mass flow. Therefore, the stall limit of a cascade in an unsteady environment is not determined solely by local inlet parameters. It appears obvious that disturbances from other cascades have to be considered.

Phase correlation between the mass flow rate and the stage pressure ratio was studied, but no clear correlation was found. Disturbances propagating axially inside the compressor largely influenced the unsteady cascade characteristic. Consequently, the effect of such disturbances must be considered when predicting unsteady performance.

These results can only be achieved from simulating the entire surge process. For this reason, the present simulation provides new insight with regard to surge phenomena.

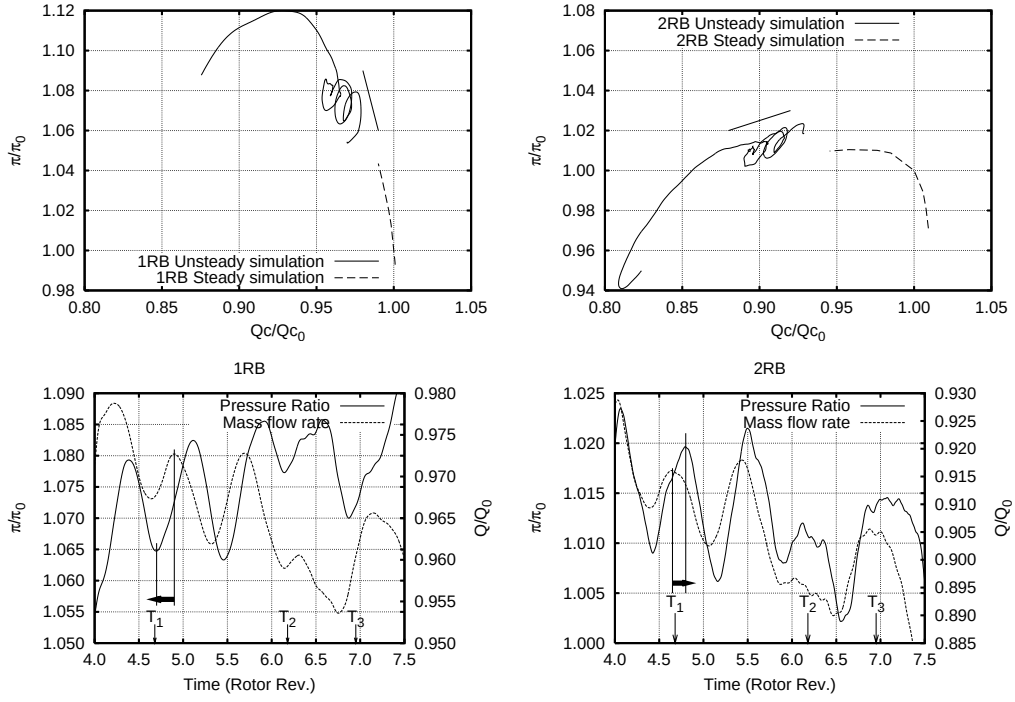

(a) 1RB

(b) 2RB

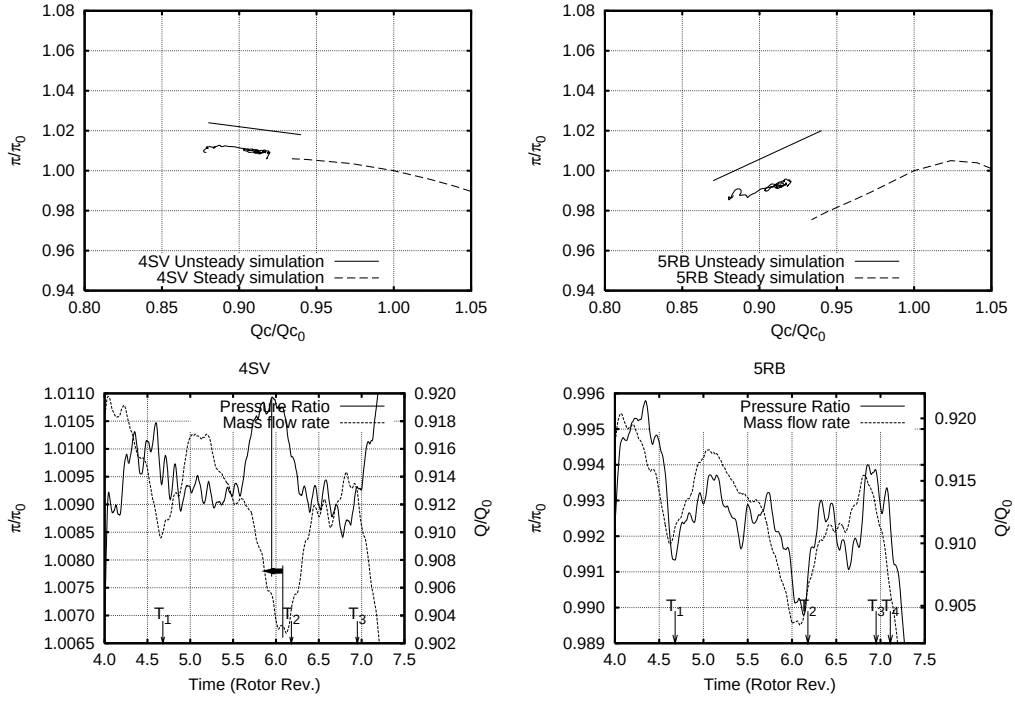

(c) 4SV

(d) 5RB

FIGURE 11. Pressure ratio - mass flow delay.

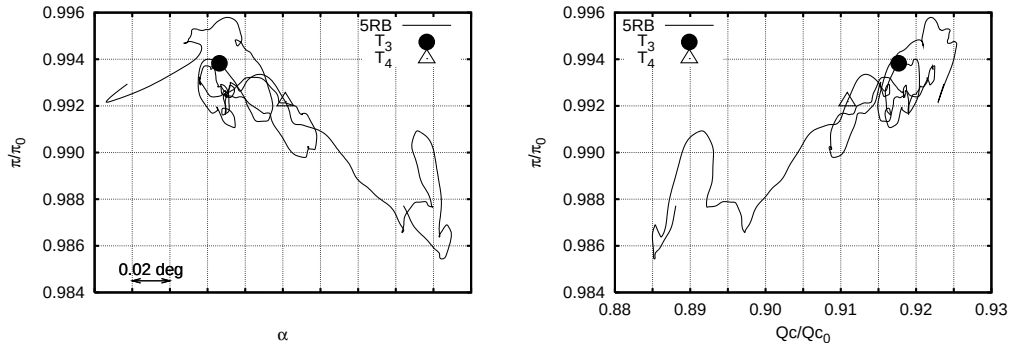

(a) relative flow angle - pressure ratio. (b) mass flow rate - pressure ratio.

FIGURE 12. 5RB stall limit.

Acknowledgments

I am thankful to Professor Moin for accepting me as a visiting fellow. I am extremely grateful to the center for bearing a portion of the expenses incurred during my stay and for providing the computing time. I also thank Pratt & Whitney for providing the geometry through the center.

REFERENCES

CAMP, T. R. & DAY, I. J. 1998 A study of spike and modal stall phenomena in a low-speed axial compressor. *Journal of Turbomachinery* 120, 393–401.

DAY, I. J. 1993 Active suppression of rotating stall and surge in axial compressors. *Journal of Turbomachinery* 115, 40–47.

DAY, I. J. 1994 Axial compressor performance during surge. *Journal of Propulsion and Power* 10(3), 329–336.

DAY, I. J. & FREEMAN, C. 1994 The unstable behavior of low and high-speed compressors. *Journal of Turbomachinery* 116, 194–201.

GREITZER, E. M. 1976 Surge and rotating stall in axial flow compressors, parts I and II. *Journal of Engineering for Power* 98, 190–217.

HAH, C., BERGNER, J., & SCHIFFER, H.-P. 2006 Short length-scale rotating stall inception in a transonic axial compressor - criteria and mechanism. In *ASME Turbo Expo 2006* number GT2006-90045.

MEDIC, G., YOU, D., KALITZIN, G., HERRMANN, M., HAM, F., PITSCH, H., VAN DER WEIDE, E., & ALONSO, J. 2007 Integrated computations of an entire jet engine. In *ASME Turbo Expo 2007* number GT2007-27094.

MOORE, F. K. & GREITZER, E. M. 1986 A theory of post-stall transients in axial compression systems I and II. *Journal of Engineering for Gas Turbines and Power* 108, 68–76 & 231–239

PADUANO, J. D., GREITZER, E. M., & EPSTEIN, A. H. 2001 Compression system stability and active control. *Annual Review of Fluid Mechanics* 33, 491–517.

SASAKI, I. & TAKATA, H. 1981 Rotating stall in blade rows operating in shear flow (2nd report: The case of shear flow with piecewise linear velocity profile). *Bulletin of JSME* 24 (198), 2074–2081.

Sekido, T., Sasaki, I., & Takata, H. 1984 Rotating stall in blade rows operating in shear flow (1st report: The case of shear flow with linear velocity profile). *Bulletin of JSME* 27 (225), 411–418.